Molecular basis for DarT ADP-ribosylation of a DNA base

Marion Schuller[1], Rachel E. Butler[2], Antonio Ariza[1], Callum Tromans-Coia[1], Gytis Jankevicius[1,3], Tim D. W. Claridge[4], Sharon L. Kendall[5], Shan Goh[5] and Graham R. Stewart[2,*], Ivan Ahel[1,*]

[1]*Sir William Dunn School of Pathology, University of Oxford, Oxford OX1 3RE, United Kingdom*

[2]*Department of Microbial Sciences, School of Biosciences and Medicine, University of Surrey, Guildford, Surrey GU2 7XH, United Kingdom*

[3]*Biozentrum, University of Basel, Basel CH - 4056, Switzerland*

[4]*Department of Chemistry, Chemistry Research Laboratory, University of Oxford, Oxford OX1 3TA, United Kingdom*

[5]*Centre for Emerging, Endemic and Exotic Disease, Pathology and Population Sciences, The Royal Veterinary College, Hawkshead Lane Hatfield Hertfordshire AL9 7TA, United Kingdom*

[*]Correspondence: ivan.ahel@path.ox.ac.uk; g.stewart@surrey.ac.uk

Supplementary Information

SI-Guide

Supplementary Discussion

DarT's position in the ART family

Over all the years of ART research, only a few examples have been reported which capture an ART in complex with its ADP-ribosylated target. These include the exotoxin A from *Pseudomonas aeruginosa* in complex with the eukaryotic translation elongation factor 2 (eEF2), which provided insights into the N-glycosidic ADPr-linkage to the diphthamide target residue in eEF2[1], and the *Clostridium perfringens* iota-toxin (Ia)–actin complex, revealing mechanistic details behind arginine ADP-ribosylation and for a general strain-alleviation model of ADP-ribosylation[2,3]. DarT presents the first example of a PARP-like ART captured in pre- and post-reaction states with a ssDNA target, which also allowed us to structurally visualise an ADP-ribosylated DNA product for the first time. DarT of *Thermus* sp. 2.9 proved to be an ideal model ART for these crystallographic studies due to its ability to generate high-resolution structures of up to 1.29 Å (unprecedented for an ART enzyme) and the fact that it is amenable for crystallisation of different states (partially and fully substrate- as well as product-bound) in the same crystal form, which limits differences due to crystal packing and grants comparability among them.
DarT is part of the first and so far only TA system characterised for reversible DNA ADP-ribosylation[4] and appears to combine several characteristics of different ADP-ribosyltransferases, giving it a unique position in the ART family. In its function as a DNA ADP-ribosylating toxin, it resembles toxins of the cholera-toxin like ADP-ribosyltransferase ('ARTC') subclass including the pierisin family and CARP-1 which are either also of bacterial origin or eukaryotic variants found in butterfly larvae or some shellfish species. These enzymes are characterised for inducing toxicity by irreversibly - in contrast to DarT - ADP-ribosylating nucleic acids, i.e. guanine bases in double-stranded DNA (dsDNA) or guanidine-derived nucleosides[5–8]. Yet, the structural features of DarT classify it within the ARTD family with close ties to PARP family members, some of which have been shown *in vitro* to be capable of nucleic acid ADP-ribosylation, yet with the phosphorylated ends of DNA and RNA as targets of this modifcation[9–13]. The only so far identified ART also encoded within a bacterial TA system is ParT, an ARTD family member with ARTC-class features, which has protein instead of DNA target specificity and is of simpler architecture when compared to DarT[14]. Furthermore, the thymine N3-ADPr linkage established by DarT represents a novel DNA damage mark, regulating metabolism by specifically modifying ssDNA elements. Thereby, it is different to not only the known thymidine modifications catalysed by bacteriophages (which are attached to the pyrimidine C5)[15] but also to known N-glycosidic ADPr-linkages to protein residues (lysine, arginine or diphthamide) or guanine nucleotides catalysed by ARTs (Supplementary Figure 4). The latter link the NAM ribose electrophilic C1 either to amino groups or to the sp^2 imidazole N3 over their lone electron pairs[16]. The ADP-ribose attachment to thymine N3, however, requires proton abstraction prior to linkage, which we propose is catalysed by DarT through an active site arginine, which presents, to our knowledge, a mechanism not described for an ART so far. In DarT, the active site arginine is an essential catalytic residue in addition to the catalytic glutamate that is conserved among the majority of ARTs. The importance of the glutamate for ADP-ribosylation catalysis is well-known and ARTs lacking the acidic residue itself substitute it from their substrate through a process termed substrate-assisted catalysis[17]. Our studies have shown that the glutamate in DarT is not an absolute requirement for the catalytic reaction. Yet, only the presence of both the arginine and the glutamate (with their potential interplay) grants the efficiency of the ADP-ribosylation reaction, resulting in cellular toxicity of DarT, and are therefore catalytically defining this transferase. Interestingly, despite having an ARTD-like fold, DarT does not show conservation of all general class-defining motif residues [H-Y-E] and displays a different arrangement of the active site residue coordinating with π-π stacking of the NAM moiety (Extended Data Figure 8A). This may be indicative

of an earlier evolution of DarT or an acquired adaption to its specialised function as DNA ADP-ribosyltransferase.

Our DarT study also enables us to understand the similarity within this family from a different perspective, which considers more than the classifying motif residues characterised so far. ARTs seem to share the spatial position and orientation of mechanistically relevant residues (Extended Data Figure 8B) even when they have completely different functions and targets. It is striking that the thymine-coordinating H119 in DarT (which is essential for DNA ADP-ribosylation) takes spatially the same position as Y375 in the iota-toxin (Ia) which was suggested to have a role in target protein, i.e. actin, recognition[3]. Both, Y375 and H119, are accommodated in the 'ARTT' loops, which do not show any similarity in either residue length or structural makeup. Furthermore, the approximate position of DarT H119 is occupied by E284 of HPF1 in the HPF1-PARP complex, whereby HPF1 sits on the 'ARTT' loop of PARP. This leads to the formation of a composite active site with the catalytic glutamate residues E284 and E545 supplied by both binding partners for catalysing serine ADP-ribosylation[18]. This ultimately provides insights into evolution of substrate specificities of PARPs required for mediating their respective function in a specific physiological context and which is still poorly understood to date. In summary, the molecular structures of DarT presented herein provide not only new mechanistic insights in DNA substrate recognition and ADP-ribosylation by an ART, which could further be exploited for site-specific DNA manipulation to induce genotoxic stress in therapeutic or biotechnological approaches, but also present us with new aspects to consider in future studies of ART function, evolution and target specificity.

Mode of NAD^+ binding by DarT

Prior to catalysing DNA ADP-ribosylation, DarT binds its NAD^+ substrate with key interactions resulting in a binding mode of constrained conformation (Extended Data Figure 5A,C): The adenine moiety is stabilised by hydrogen bonding to the K28 and L30 backbone amides, the adenine-proximal ribose bonds with its 2' and 3' hydroxyl groups to T15/H13 and N19, respectively, while the NAM moiety is fixed in position by π-π interaction with Y71 and hydrogen bonding of its primary amide to I14 and intramolecularly to the beta-phosphate. The ADP-ribosylation reaction catalysed by ARTs generally proceeds via the S_N1 mechanism[19,20]. Constraining the NAD^+ molecule is thereby important, promoting NAD^+ cleavage which subsequently generates the reactive oxocarbenium ion as an intermediate for nucleophilic attack of the respective target, while leaving NAM as a reaction by-product[20]. Interestingly, the NAD^+-stabilising interactions are not made directly to the loop-helix region, including the 'donor loop', explaining its flexibility even after NAD^+-binding. However, the loop-helix region still provides protection for the reactive oxocarbenium ion from reacting with water or nucleophiles other than its target (Extended Data Figure 1D). Furthermore, when compared to DNA-binding, the NAD^+ is bound within a large pocket involving a water network for its coordination which may also permit the flexibility required for the flip of the oxocarbenic NAM ribose, induced by strain-alleviation, after NAD^+ cleavage to connect with the thymine. The resulting slightly 'looser' binding mode, compared to DNA-binding, is also reflected in the lower binding affinity of DarT to NAD^+ (K_D = 58 µM) compared to the ADP-ribosylated DNA (K_D = 961 nM), as determined by calorimetric measurements (Figure 2E, Extended Data Figure 5D, Supplementary Figure 3).

The catalytic mechanism of DarT

A coordinated action of several residues in the active site is important for DNA ADP-ribosylation catalysis (Figure 3A, B), which includes: (i) locking of the thymidine base in plane for reaction, (ii) polarisation of the NAD^+ molecule for cleavage, (iii) stabilisation of the oxocarbenium ion and (iv) proton abstraction from N3 of the thymidine base to enable the ADPr-linkage.

Thymine coordination is predominantly contributed by H119 (accommodated in the 'ARTT' loop) through its hydrogen bonding with the base C2 carbonyl group. The mechanistic relevance of H119 was confirmed by both conservation analysis among the DarT family (Extended Data Figure 4B) and mutagenesis studies (Figure 3C,D). Restraining and polarising the NAD^+ molecule over the bond between ribosyl C1" and NAM N1 is essential for its cleavage and generation of the oxocarbenium ion as intermediate for the S_N1-type reaction. The highly conserved Y71 is involved in this process through NAM π-π interaction, with its hydroxyl group having additional effects on bond polarisation (Figure 3A,D, Extended Data Figure 4B, 5C). Mutagenesis studies showed the general dispensability of Y71 for the mechanism but essentiality for efficient catalysis (Figure 3C,D). NAD^+ polarisation in ARTs is generally mediated by interaction of the 2" hydroxyl group of the NAM ribose with the conserved, ART-characterising catalytic glutamate residue[19–21]. Based on modelling results, the catalytic E160 in DarT is noticeably more distant from (> 4 Å) and at a non-ideal angle to the ribose 2" hydroxyl group but could nevertheless potentially promote C1"-ribose – N1 NAM polarisation due to overall proximity to this bond. As in other ARTs, E160 is completely conserved among the DarT family and is essential for the mechanism, as was confirmed by mutagenesis studies (Figure 3C,D, Extended Data Figure 4B). Interestingly, the NAD^+-bound structure of DarT revealed that the 2" hydroxyl group of the NAM ribose is instead well-coordinated by hydrogen-bonding to ε-NH of R51 (Figure 3B). R51 is equally well-conserved as E160 (Extended Data Figure 4B) and its presence appears mechanistically essential since both R51A and R51K mutation result in loss of toxicity and ADP-ribosylation activity (Figure 3C,D). This further suggests that it is the arginine guanidinium group with its unique physicochemical properties that is required for catalysing DNA ADP-ribosylation. With R51's close and ideal position to the 2" hydroxyl group, it could therefore be involved in NAD^+ polarisation. Interestingly, closer analysis of R51 also revealed the high flexibility of its side-chain, allowing it to adopt different and well-defined orientations in the *apo* and substrate-and product-bound states (Figure 3A, Extended Data Figure 3E). NAD^+-binding orientates R51 to the NAM ribose and upon DNA-binding R51 slightly re-orientates again, clearly facing the N(3)-H of the thymidine base (Extended Data Figure 3E). This suggests that R51 could function in the DarT mechanism as a catalytic base responsible for the proton abstraction of the thymine N3. The resulting nucleophilic N3 enables linkage from the DNA base to the electrophilic ribose C1" of the oxocarbenium ion produced upon NAD^+ cleavage. The required prior deprotonation and pK_a lowering of R51 may be a consequence of a potential interaction with E160, as has been observed for other unrelated enzymes which use arginine as a base[22] (Extended Data Figure 3D). Finally, the DarT-conserved M78 could also be identified to contribute to catalysis (Figure 3C,D, Extended Data Figure 4B). As its flexible side-chain finds a fixed orientation upon NAD^+-binding, likely through weak interaction with the positive charge over NAM N1, M78 may also function to stabilise the positive charge over the oxocarbenium ion[23]. Altogether, this allows to suggest a catalytic mechanism for DNA ADP-ribosylation by DarT, as shown in Figure 3E.

NMR analysis of DarT ADP-ribosylated DNA

The newly identified connectivity between the ADP-ribose and the ssDNA was established in solution by the use of 2D NMR techniques. New resonances belonging to the substituted ADP-ribose fragment were identified through comparison of the ^{1}H NMR and ^{1}H-^{13}C HSQC spectra of the modified *versus* the parent ssDNA data (Supplementary Figure 2-1 A, B), with the ribose protons subsequently assigned from selective 1D TOCSY data (Supplementary Figure 2-1 C). The connection of the ribose to the thymine base in ssDNA was identified from the observation specific through-bond ^{1}H-^{13}C correlations in the HMBC experiment. Thus, the ribose H1" proton at 6.37 ppm was observed to correlate to carbon resonances at 151.1 and 164.8 ppm. That at 151.1 ppm belonged to the thymidine C2 carbon, as evidenced by correlations from T-H6 and T-H1', whilst that at 164.8 ppm could be assigned to thymidine C4, for which additional correlations arise from T-H6 and T-Me5 protons (Supplementary Figure 2-2 A, bottom). The corresponding correlations within the thymidine ring were also apparent in the parent ssDNA HMBC spectra (Supplementary Figure 2-2 A, top) confirming the identification of these carbon centres. The HMBC data of the modified ssDNA therefore provided unequivocal evidence for the newly formed bond to occur between the ribose C1" and the thymidine N3 (Supplementary Figure 2-2 C, left). The stereochemistry at the newly formed connection was explored through consideration of ^{1}H J_{HH} coupling constants and through-space nOes (Supplementary Figure 2-2 C, right). The relatively large H1"-H2" coupling constant of 6.7 Hz is consistent with a *syn* relationship which is supported by the clear dominance of the H1"-H2" nOe observed in 1D ROESY spectra (Supplementary Figure 2-2 B). The new connectivity therefore adopts the α-configuration.

Supplementary Figure 1

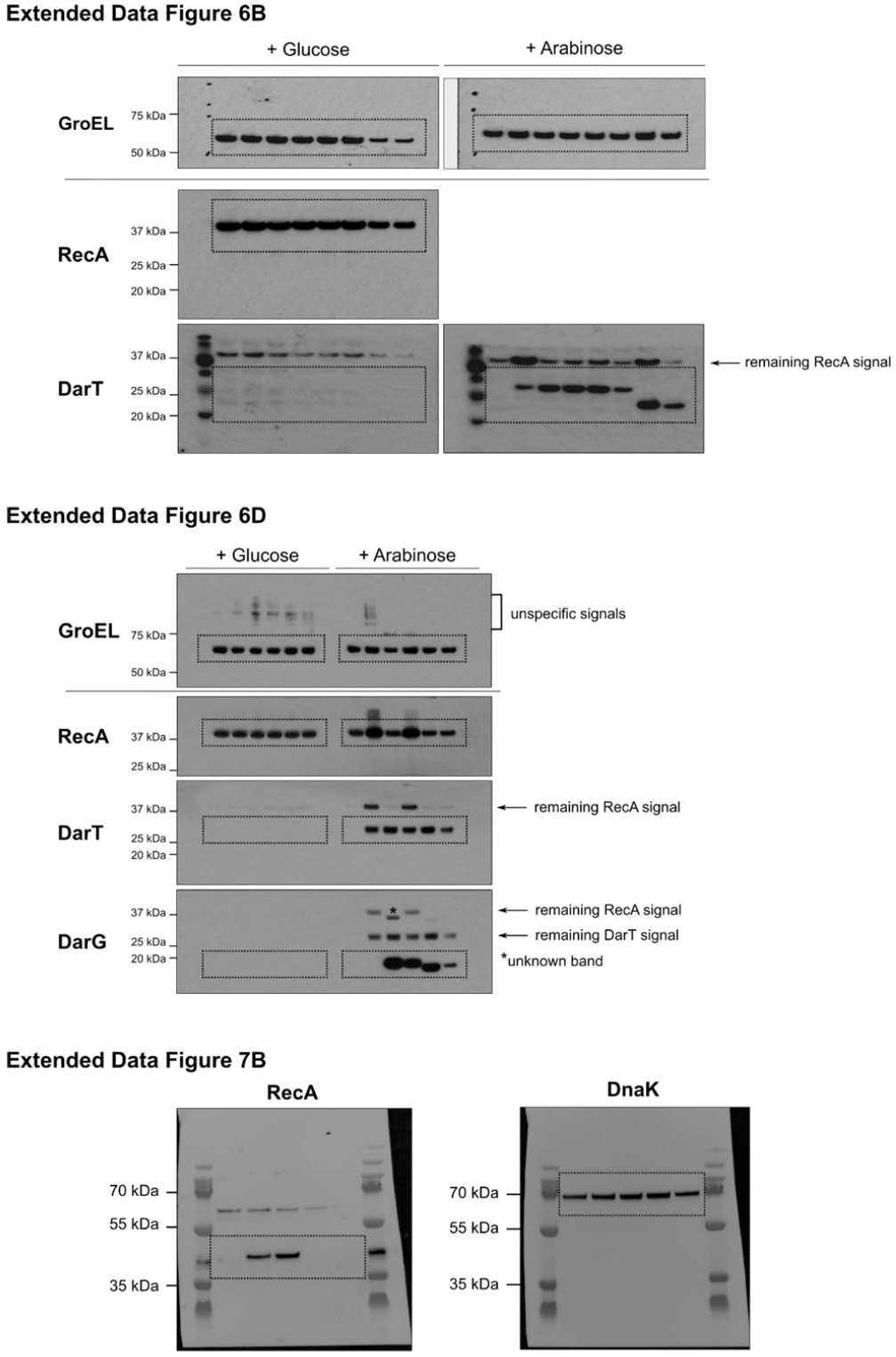

Supplementary Figure 1-1. Uncropped figure data of protein immunoblots shown in the manuscript. Cropped images for figures are indicated by a dotted box. All markers including the loading controls, GroEL and DnaK, were detected together on one processed gel/blot. A horizontal line between markers indicates cutting of the Western blot membrane for the immunoblotting procedure.

Extended Data Figure 6B

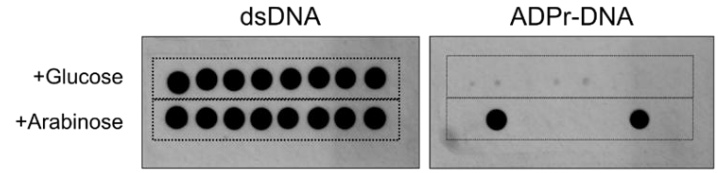

Extended Data Figure 6D

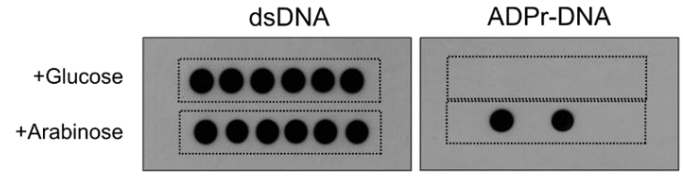

Extended Data Figure 6E

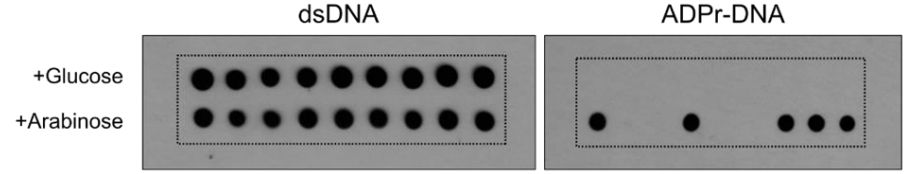

Figure 4A

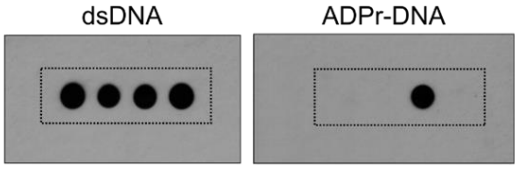

Figure 4B

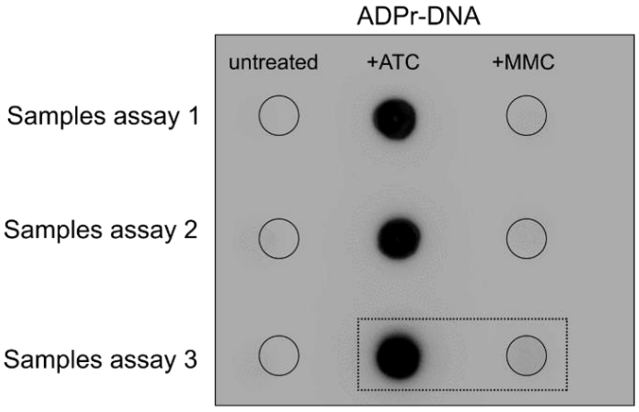

Extended Data Figure 6A

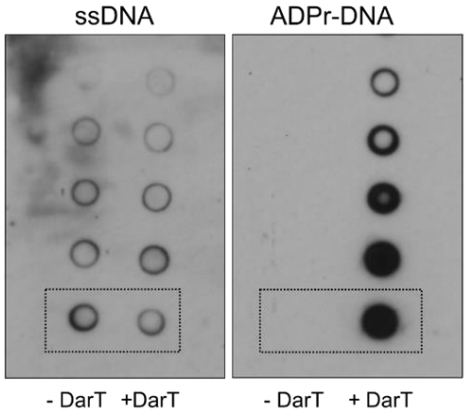

Supplementary Figure 1-2. Uncropped figure data of dot blot assays shown in the manuscript. Cropped images for figures are indicated by a dotted box.

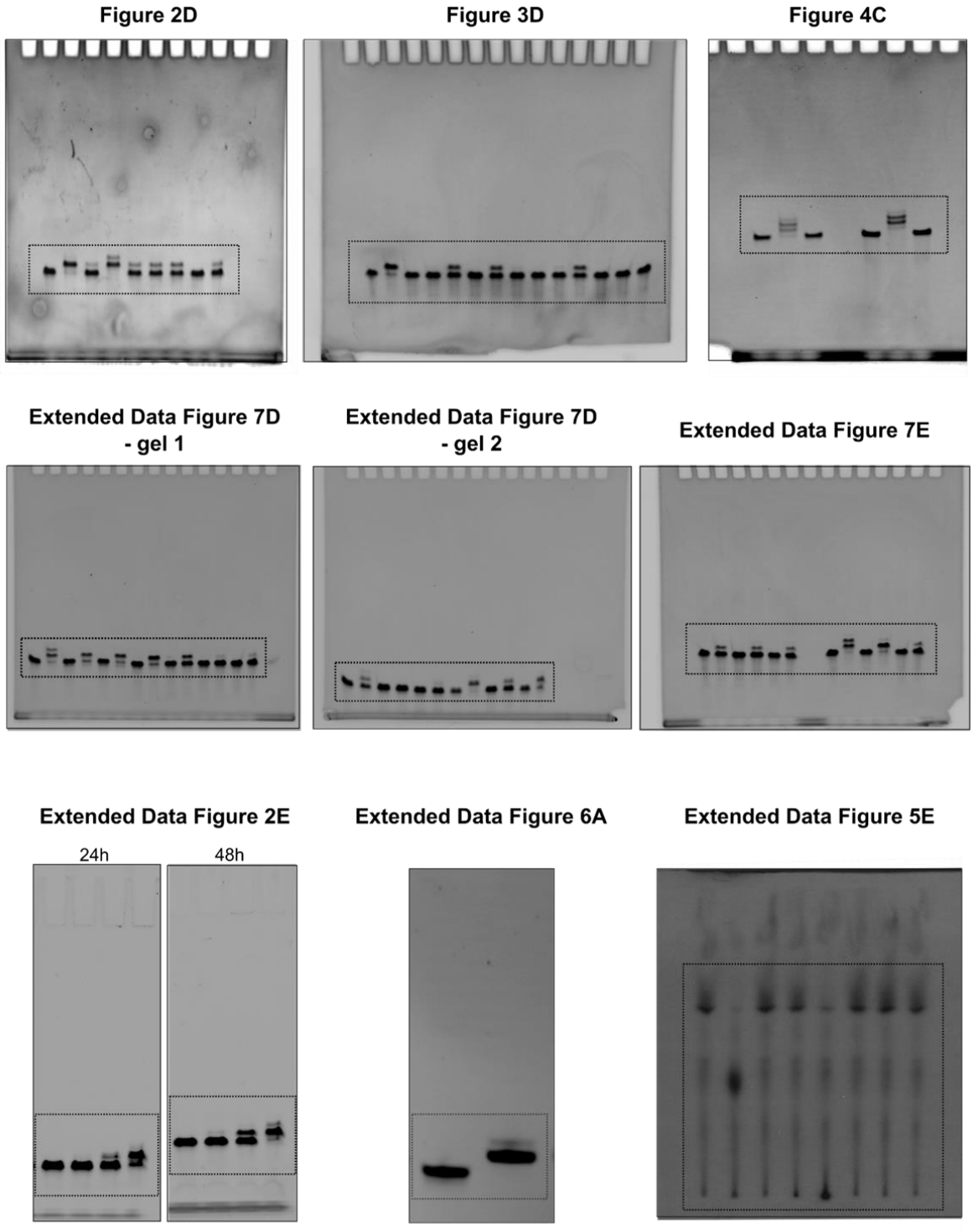

Supplementary Figure 1-3. Uncropped figure data of activity assays shown in the manuscript. Cropped images for figures are indicated by a dotted box. Figure 2G shows the autoradiography of a TLC plate analysing the reaction products for testing NADase activity of DarT while all other images show *in vitro* ADP-ribosylation activity assay results by visualising the modification of the oligos under UV light after separation and ethidium bromide-staining of the reaction products on denaturing polyacrylamide gel.

Supplementary Figure 2

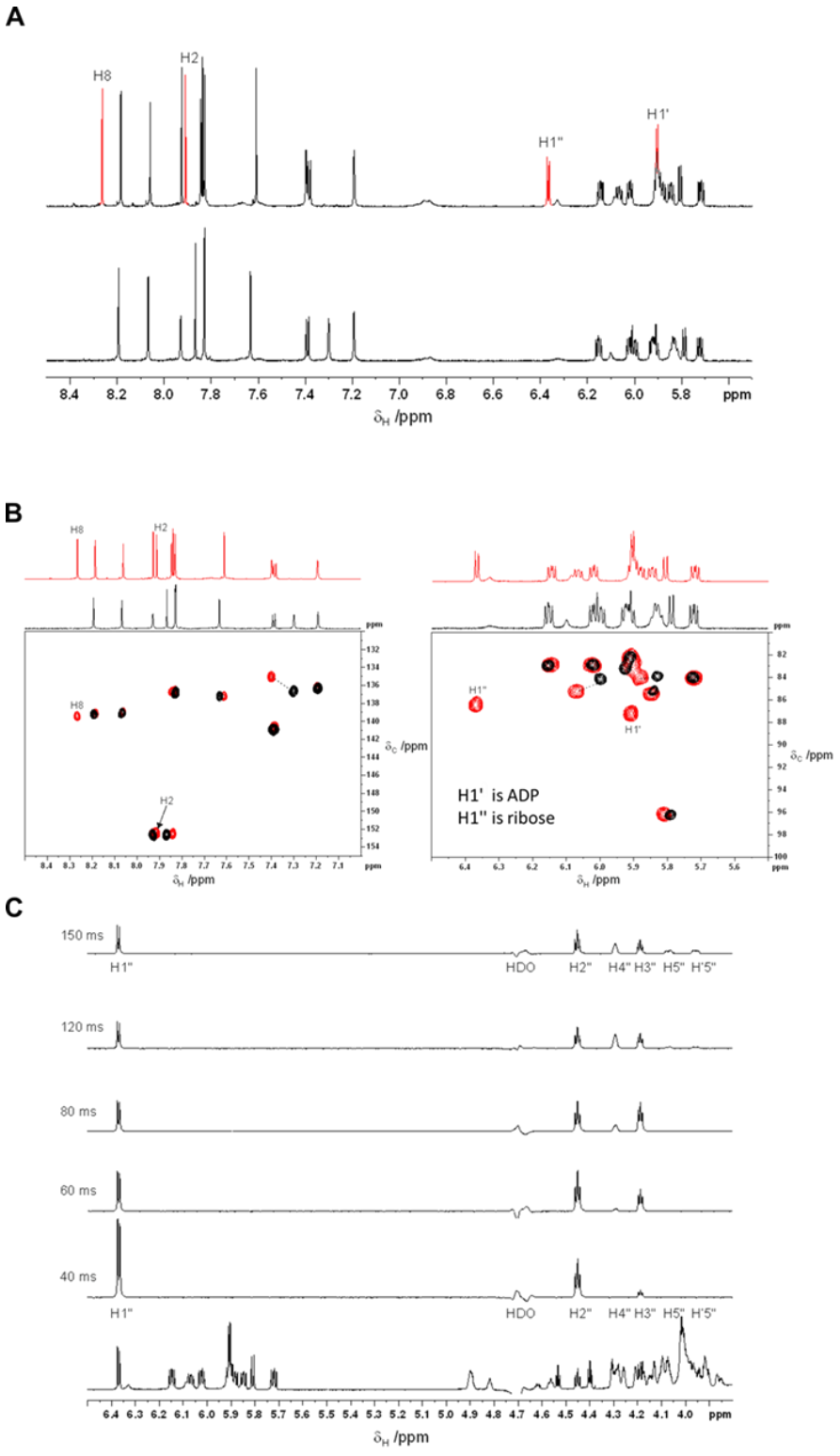

Supplementary Figure 2-1 [related to Figure 1D]. NMR analysis of ADP-ribosylated DNA – identification of ribose resonances attached to DNA strand. (A) Overlay of the partial ^{1}H NMR spectra of modified ssDNA (**top**) and parent ssDNA (**bottom**). Resonances highlighted in red arise from the ADP-ribose attached to the ssDNA; H1' is from the ADP moiety, H1'' from ribose, and H2 and H8 belong to the adenine ring. **(B)** Overlap of regions from ^{1}H-^{13}C HSQC spectra of parent ssDNA (black) and modified ssDNA (red). Labelled resonances arise from the added ADP-ribose fragment. **(C)** Overlay of the partial ^{1}H NMR spectrum (lower trace) and 1D TOCSY spectra (upper traces, with increasing mixing times) of the modified ssDNA identifying the resonances of the ribose sugar attached directly to the ssDNA.

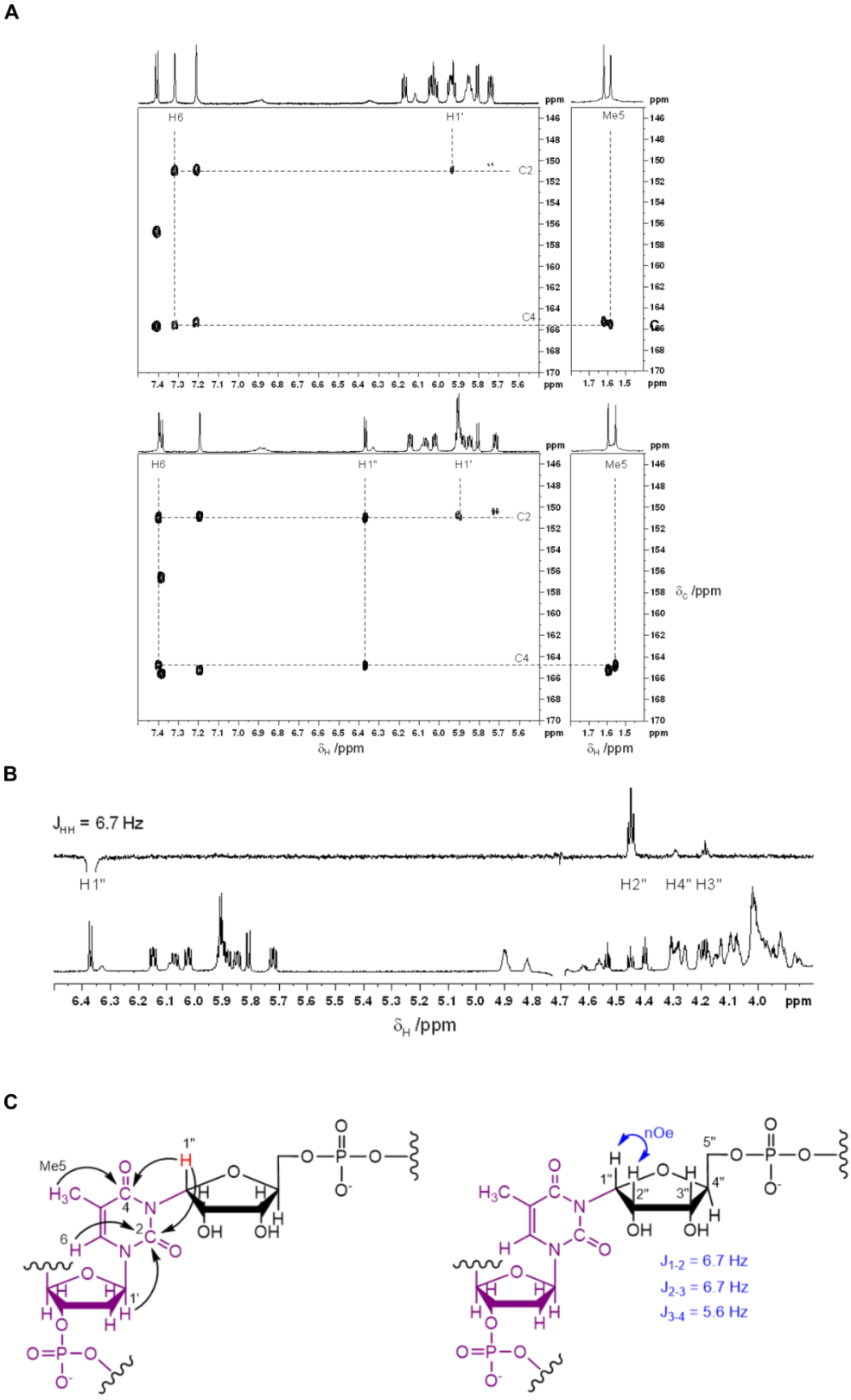

Supplementary Figure 2-2 [related to Figure 1D]. NMR analysis of ADP-ribosylated DNA – identification of the ribose-thymine connectivity and its stereo configuration. (A) Key regions from the ^{1}H-^{13}C HMBC spectra of (**top**) parent ssDNA and (**bottom**) modified ssDNA. Correlations that establish connectivity from the ADP-ribose ring to the thymidine base and those that define assignments for the thymidine ring carbons are highlighted by dashed lines. **(B)** Partial ^{1}H NMR spectrum of modified ssDNA (**bottom**) with 1D selective ROESY (**top**, τ_m = 300 ms) targeting the H1" of the modified ribose ring. **(C) (Left)** Key correlations observed in ^{1}H-^{13}C HMBC spectra establishing the connectivity between the ribose and thymine rings. **(Right)** NOe and scalar-coupling data defining the configuration at the newly formed stereocenter as α.

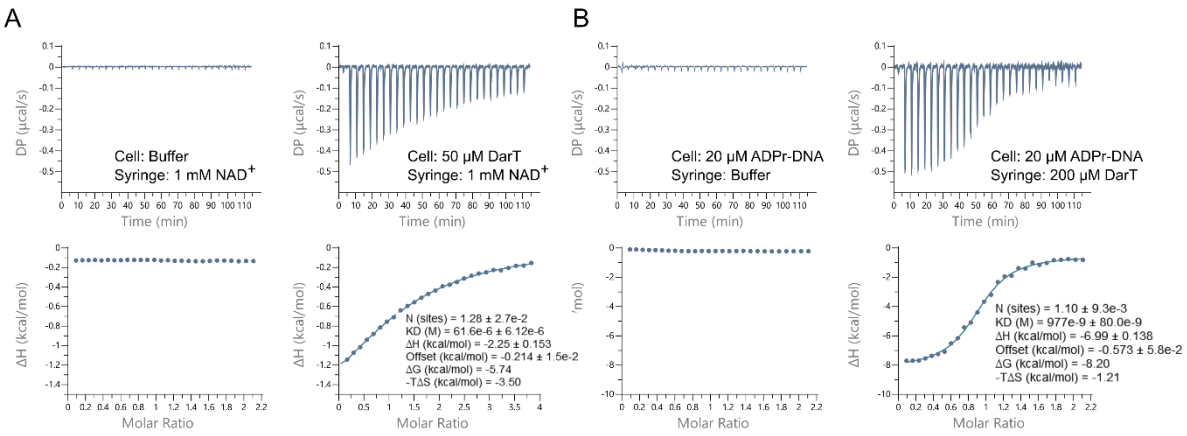

Supplementary Figure 3 [related to Figure 2E, Extended Data Figure 5D]. ITC results for determining binding parameters for *Thermus* sp. 2.9 DarT E160Q to (A) NAD$^+$ and (B) ADPr-DNA. ITC data analysis was performed with MicroCal PEAQ-ITC analysis software (Malvern). The upper part of the panels shows the raw titration curves resulting from stepwise addition of the titrant from the syringe to the calorimetric cell as indicated. NAD$^+$ binding parameters were determined with direct titration of the ligand to the DarT protein, ADPr-DNA binding parameters with reverse titration. The lower part of the panels shows the normalised binding enthalpies corrected for the heat of dilution as a function of binding site saturation. Solid lines represent a nonlinear least square fit using a single-site binding model and calorimetric parameters are given in the respective graphs. Representative graphs for three independently performed experiments are shown.

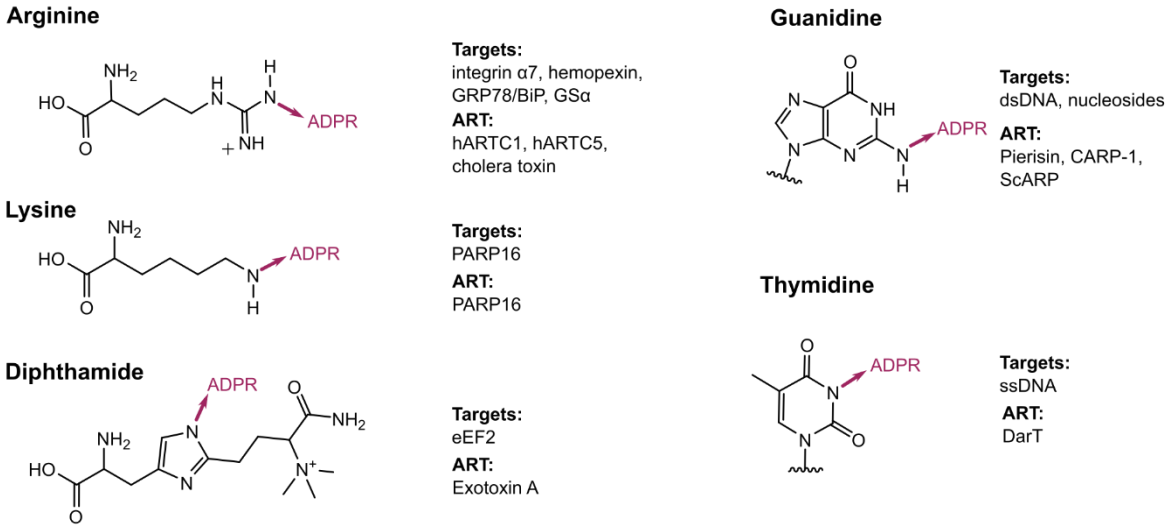

Supplementary Figure 4 [related to Supplementary Discussion] Comparison of N-glycosidic ADPr-linkages catalysed by ARTs. Examples of ADP-ribosylated targets of respective ARTs are given next to the molecular structures[16].

Supplementary Table 1. DarT substrate oligonucleotides used in this study.

Oligo-ID	Sequence (5'→3')	Purpose
DarT-ADPr-27mer	CACGACACGAGCAGGCATGTCCACGTG	ADP-ribosylation activity assay
DarT-ADPr-27mer-Cy3	Cy3-GAGCTGTACAAGTCAGATCTCGAGCTC	ADP-ribosylation activity assay
DarT-ADPr-8mer	GATGTCAG	For NMR studies
DarT-ADPr-5mer	ATGTC	For co-crystallisation and ITC studies with DarT
OriC_UpperStrand	TGTTCTTCCGACAACGTTCTTAAAAAAACTTCTCTCTC	OriC modification by *Mtb* DarT
OriC_LowerStrand	GAGAGAGAAGTTTTTTTAAGAACGTTGTCGGAAGAACA	OriC modification by *Mtb* DarT
DarT_Substrate24	CACGACACGAGCAGGCATGTCCACGTG	*Mtb* DarT motif studies
DarT_Substrate30	CACGACACGAGCAGGCATCTCCACGTG	*Mtb* DarT motif studies
DarT_Substrate35	CACGACACGAGCAGGCATGTTCACGTG	*Mtb* DarT motif studies
DarT_Substrate38	CACGACACGAGCAGGCATCTTCACGTG	*Mtb* DarT motif studies
DarT_Substrate61	CACGACACGAGCAGGCATTTACACGTG	*Mtb* DarT motif studies
DarT_Substrate62	CACGACACGAGCAGGCATTTTCACGTG	*Mtb* DarT motif studies
DarT_Substrate64	CACGACACGAGCAGGCATTTTGACGTG	*Mtb* DarT motif studies
DarT_Substrate65	CACGACACGAGCAGGCAATTTGACGTG	*Mtb* DarT motif studies
DarT_Substrate66	CACGACACGAGCAGGCAGTTTGACGTG	*Mtb* DarT motif studies
DarT_Substrate67	CACGACACGAGCAGGCACTTTGACGTG	*Mtb* DarT motif studies
DarT_Substrate68	CACGACACGAGCAGGCATATTGACGTG	*Mtb* DarT motif studies
DarT_Substrate69	CACGACACGAGCAGGCATGTTGACGTG	*Mtb* DarT motif studies
DarT_Substrate70	CACGACACGAGCAGGCATCTTGACGTG	*Mtb* DarT motif studies
DarT_Substrate71	CACGACACGAGCAGGCATTATGACGTG	*Mtb* DarT motif studies
DarT_Substrate72	CACGACACGAGCAGGCATTGTGACGTG	*Mtb* DarT motif studies
DarT_Substrate73	CACGACACGAGCAGGCATTCTGACGTG	*Mtb* DarT motif studies
DarT_Substrate74	CACGACACGAGCAGGCATTTAGACGTG	*Mtb* DarT motif studies
DarT_Substrate75	CACGACACGAGCAGGCATTTGGACGTG	*Mtb* DarT motif studies
DarT_Substrate76	CACGACACGAGCAGGCATTTCGACGTG	*Mtb* DarT motif studies

Supplementary Table 2. Primer sequences used for experimental procedures.

Oligo-ID	Sequence (5'→3')	Purpose	Comment
Rv59UPF	GCGTACTAGTACCGCGTCCACCAGAATCTT	Δ*darTG* strain generation	---
Rv59UPR	GCGTACTAGTGGTGATCATGCATTAGTCCC	Δ*darTG* strain generation	---
Rv60DF	GCGTTCTAGAATCGGTGTTGCCCTCGACCG	Δ*darTG* strain generation	---
Rv60DR	GCGTTCTAGACACCAGTTGAGCGGGGCGTC	Δ*darTG* strain generation	---
P232_pET_F	AACTTTAAGAAGGAGATATACCATG	DH5α-macro generation	---
P233_peET_R	CATGCATCTCGAGGCATGCCTTTGTTAGC AGCCGGATCTC	DH5α-macro generation	---
P238_link_pOSIP	ATAAACTGCCAGGAATTGGGGATCGTTGA CGGCTAGCTCAGTCCTAGGTACAGTGCTAG CTAACTTTAAGAAGGAGATATACCATG	DH5α-macro generation	---
darG_Forward	GGGACATCACCCCAACACAGTTGA	*darG* CRISPRi	The first four bases of the primers (underlined) are used for cloning the sgRNA into pRH2521.
darG_Reverse	AAACTCAACTGTGTTGGGGTGATG	*darG* CRISPRi	
OriC_5F	GCGCTAGCACGGCGTGTTCT	ADPr-IP	Efficiency: 98.6%
OriC_5R	ACGGAACCGCCGGGACTGTA	ADPr-IP	Efficiency: 98.6%
Rv2129_PF	GTAACGAGCACTTCGCCAAC	ADPr-IP	Efficiency: 95.5%
Rv2129_PR	CAGGTCGGCCTTGGTATCG	ADPr-IP	Efficiency: 95.5%
Rv0058_3F	CCAGTAGGCGTCTCATCGAC	Transcriptional linkage *dnaB-darTG*, RT-qPCR	Targets *dnaB*
Rv0058_3R	ACGTGACGAAGGAACCTGAC	Transcriptional linkage *dnaB-darTG*, RT-qPCR	Targets *dnaB*
DnaB_DarT_10F	GGGGGAGAAGCGGATTTCAT	Transcriptional linkage *dnaB-darTG*	Targets *dnaB – darT* junction
DnaB_DarT_10	GAGATTGTCGGCATGGGTGA	Transcriptional linkage *dnaB-darTG*	Targets *dnaB – darT* junction
Rv0059_5F	TCGTCGACTTTGACCTGCTC	Transcriptional linkage *dnaB-darTG*, RT-qPCR	Targets *darT*
Rv0059_5R	GTTCGTACCCGTGTCATCGT	Transcriptional linkage *dnaB-darTG*, RT-qPCR	Targets *darT*
DarT_DarG_3 F	TCGTCGACTTTGACCTGCTC	Transcriptional linkage *dnaB-darTG*	Targets *darT-darG* junction
DarT_DarG_3R	CGTTTGCACGCCTTTTCGTA	Transcriptional linkage *dnaB-darTG*	Targets *darT-darG* junction
Rv0060_6F	TACGAAAAGGCGTGCAAACG	Transcriptional linkage *dnaB-darTG*, RT-qPCR	Targets *darG*
Rv0060_6R	GCGTCGATATAGGCCAGCTT	Transcriptional linkage *dnaB-darTG*, RT-qPCR	Targets *darG*
RecA_F	AATGACCGGCGCGCT	RT-qPCR	Targets *recA*[24]
RecA_R	CGCGGAGCTGGTTGATG	RT-qPCR	Targets *recA*[24]
DnaE2_F	CCGGTGGAATGGGCG	RT-qPCR	Targets *dnaE*[24]
DnaE2_R	AATTTCACCAAGCCGATTGC	RT-qPCR	Targets *dnaE*[24]
sigA_F	GACGAGGAGATCGCTGAACC	RT-qPCR	Targets *sigA*[24]
sigA_R	TCGTCTTCATCCCAGACGAAA	RT-qPCR	Targets *sigA*[24]

Supplementary Table 3. Strains and plasmids used in this study.

Strain or plasmid-ID	Description	Source
Escherichia coli		
DH5α	*huA2 a(argF-lacZ)U169 phoA glnV44 a80a(lacZ)M15 gyrA96 recA1 relA1 endA1 thi-1 hsdR17*	NEB
DH5α-macro	DH5α with integrated *Thermus aquaticus* DarG macrodomain at P21 site	This study
BL21	*fhuA2 [lon] ompT gal [dcm] ΔhsdS*	NEB
BL21(DE3)	*fhuA2 [lon] ompT gal (λ DE3) [dcm] ΔhsdS λ DE3 = λ sBamHIo ΔEcoRI-B int::(lacI::PlacUV5::T7 gene1) i21 Δnin5*	NEB
Rosetta™ BL21 (DE3)	*F-ompT hsdSB(rB- mB-) gal dcm (DE3) pRARE* (cam^R)	Novagen
***Mycobacterium* spp.**		
Mycobacterium bovis BCG	BCG / Pasteur 1173P2	Lab stocks
M. tuberculosis GC1237	*Mycobacterium tuberculosis* strain of the Beijing genotype	Caminero *et al.*, 2001[25]
M. tuberculosis ΔdarTG	*M. tuberculosis* GC1237 *ΔdarTG::hyg*	This study
Plasmids		
pOSIP-KT	Plasmid for gene integration at P21 site	Addgene[26]
pRH2502	Integrative plasmid derived from pTC-0X-1L, expressing $dCas9_{Spy}$ from an inducible tetRO promoter (uv15tetO)	Singh *et al.*, 2016[27]
pRH2521	Non- integrative plasmid derived from pTE-10M-0X, expressing sgRNA from an inducible tetRO promoter (Pmyc1tetO)	Singh *et al.*, 2016[27]
pBAD33	Medium copy plasmid with an arabinose-inducible promoter; cam^R	Guzman *et al.*, 1995[28]
pET28a	Medium copy plasmid containing the IPTG-inducible promoter; kan^R	Invitrogen
pNIC28-Bsa4	Medium copy plasmid containing the IPTG-inducible promoter; kan^R	Addgene[29]
pBAD33_Taq_*darT*	pBAD33 carrying *Thermus aquaticus darT* full-length; cam^R	Jankevicius *et al.* 2017[4]
pBAD33_Taq_*darT*^{E160A}	pBAD33 carrying *Thermus aquaticus darT*^{E160A} full-length; cam^R	Jankevicius *et al.* 2017[4]
pET28_Taq_*darG*	pET28a carrying *Thermus aquaticus darG* full-length; kan^R	Jankevicius *et al.* 2017[4]
pBAD33_EPEC_*darT*^{G49D}	pBAD33 carrying EPEC *darT*^{G49D} full-length; cam^R	Lawarée *et al.* 2020[30]
pBAD33_EPEC_*darT*^{E170A}	pBAD33 carrying EPEC *darT*^{E170A} full-length; cam^R	Lawarée *et al.* 2020[30]
pET28_Taq_*darG*_macro	pET28a carrying *Thermus aquaticus darG* macrodomain (aa 1-155); kan^R	Jankevicius *et al.* 2017[4]
pET28_Mtb_*darG*_macro	pET28A carrying *M. tuberculosis* macrodomain of *darG* (aa 1-155); kan^R	Jankevicius *et al.* 2017[4]
pET28_EPEC_*darG*_macro	pET28A carrying EPEC macrodomain of *darG* (aa 1-113); kan^R	Lawarée *et al.* 2020[30]
pSG_darG	sgRNA targeting between +62bp to +82bp (not including the 3nt PAM) downstream of the *darG* start codon cloned into pRH2521	This study
pBAD33_Taq_*darT*^{Y47A}	pBAD33 carrying *Thermus aquaticus darT*^{Y47A} full-length; cam^R	This study
pBAD33_Taq_*darT*^{Y47F}	pBAD33 carrying *Thermus aquaticus darT*^{Y47F} full-length; cam^R	This study
pBAD33_Taq_*darT*^{H49A}	pBAD33 carrying *Thermus aquaticus darT*^{H49A} full-length; cam^R	This study
pBAD33_Taq_*darT*^{H53A}	pBAD33 carrying *Thermus aquaticus darT*^{H53A} full-length; cam^R	This study
pBAD33_Taq_*darT*^{R54A}	pBAD33 carrying *Thermus aquaticus darT*^{R54A} full-length; cam^R	This study
pBAD33_Taq_*darT*^{R54K}	pBAD33 carrying *Thermus aquaticus darT*^{R54K} full-length; cam^R	This study
pBAD33_Taq_*darT*^{H68A}	pBAD33 carrying *Thermus aquaticus darT*^{H68A} full-length; cam^R	This study
pBAD33_Taq_*darT*^{Y74S}	pBAD33 carrying *Thermus aquaticus darT*^{Y74S} full-length; cam^R	This study

pBAD33_Taq_*darT*^{Y74F}	pBAD33 carrying *Thermus aquaticus darT*^{Y74F} full-length; cam^{R}	This study
pBAD33_Taq_*darT*^{R78A}	pBAD33 carrying *Thermus aquaticus darT*^{R78A} full-length; cam^{R}	This study
pBAD33_Taq_*darT*^{M81A}	pBAD33 carrying *Thermus aquaticus darT*^{M81A} full-length; cam^{R}	This study
pBAD33_Taq_*darT*^{Y83A}	pBAD33 carrying *Thermus aquaticus darT*^{Y83A} full-length; cam^{R}	This study
pBAD33_Taq_*darT*^{H122A}	pBAD33 carrying *Thermus aquaticus darT*^{H122A} full-length; cam^{R}	This study
pBAD33_Taq_*darT*^{R154A}	pBAD33 carrying *Thermus aquaticus darT*^{R154A} full-length; cam^{R}	This study
pBAD33_Taq_*darT*^{R154W}	pBAD33 carrying *Thermus aquaticus darT*^{R154W} full-length; cam^{R}	This study
pBAD33_Taq_*darT*^{Q158A}	pBAD33 carrying *Thermus aquaticus darT*^{Q158A} full-length; cam^{R}	This study
pBAD33_Taq_*darT*^{E160D}	pBAD33 carrying *Thermus aquaticus darT*^{E160D} full-length; cam^{R}	This study
pBAD33_Taq_*darT*^{E160Q}	pBAD33 carrying *Thermus aquaticus darT*^{E160Q} full-length; cam^{R}	This study
pBAD33_Tsp2.9_*darT*^{E160Q}	pBAD33 carrying *Thermus* sp. 2.9 *darT* full-length; cam^{R}	This study
pBAD33_Mtb_*darT*	pBAD33 carrying *M. tuberculosis darT* full-length; cam^{R}	This study
pNIC28_Tsp2.9_*darT*^{E160A}	pNIC28-Bsa4 carrying *Thermus* sp.2.9 *darT*^{E160A} full-length; kan^{R}	This study
pNIC28_Tsp2.9_*darT*^{E160Q}	pNIC28-Bsa4 carrying *Thermus* sp.2.9 *darT*^{E160Q} full-length; kan^{R}	This study
pET28_Taf_*darTG*^{E152A}	pET28a with 6xHis-TEV-V5 carrying *Thermosipho africanus darTG*^{E152A} full-length; kan^{R}	This study
pET28_Taq_*darG*$^{N22A-K80A}$_macro	pET28a carrying *Thermus aquaticus darG*$^{N22A-K80A}$ macrodomain (aa 1-155); kan^{R}	This study

Supplementary References

1. Jørgensen, R. *et al.* Exotoxin A-eEF2 complex structure indicates ADP ribosylation by ribosome mimicry. *Nature* **436**, 979–984 (2005).
2. Tsuge, H. *et al.* Structural basis of actin recognition and arginine ADP-ribosylation by Clostridium perfringens ι-toxin. *Proc. Natl. Acad. Sci. U. S. A.* **105**, 7399–7404 (2008).
3. Tsurumura, T. *et al.* Arginine ADP-ribosylation mechanism based on structural snapshots of iota-toxin and actin complex. *Proc. Natl. Acad. Sci. U. S. A.* **110**, 7524–7528 (2013).
4. Jankevicius, G., Ariza, A., Ahel, M. & Ahel, I. The Toxin-Antitoxin System DarTG Catalyzes Reversible ADP-Ribosylation of DNA. *Mol. Cell* **64**, 1109–1116 (2016).
5. Takamura-Enya, T. *et al.* Mono(ADP-ribosyl)ation of 2′-deoxyguanosine residue in DNA by an apoptosis-inducing protein pierisin-1 from cabbage butterfly. *Proc. Natl. Acad. Sci. U. S. A.* **98**, 12414–12419 (2001).
6. Oda, T. *et al.* Structural basis of autoinhibition and activation of the DNA-targeting ADP-ribosyltransferase pierisin-1. *J. Biol. Chem.* **292**, 15445–15455 (2017).
7. Nakano, T. *et al.* Purification and molecular cloning of a DNA ADP-ribosylating protein, CARP-1, from the edible clam Meretrix lamarckii. *Proc. Natl. Acad. Sci. U. S. A.* **103**, 13652–13657 (2006).
8. Lyons, B., Lugo, M. R., Carlin, S., Lidster, T. & Rod Merrill, A. Characterization of the catalytic signature of Scabin toxin, a DNA-targeting ADP-ribosyltransferase. *Biochem. J.* **475**, 225–245 (2018).
9. Munnur, D. & Ahel, I. Reversible mono-ADP-ribosylation of DNA breaks. *FEBS J.* **284**, 4002–4016 (2017).
10. Munnur, D. *et al.* Reversible ADP-ribosylation of RNA. *Nucleic Acids Res.* **47**, 5658–5669 (2019).
11. Belousova, E. A., Ishchenko, A. A. & Lavrik, O. I. DNA is a New Target of Parp3. *Sci. Rep.* **8**, 1–12 (2018).
12. Zarkovic, G. *et al.* Characterization of DNA ADP-ribosyltransferase activities of PARP2 and PARP3: New insights into DNA ADP-ribosylation. *Nucleic Acids Res.* **46**, 2417–2431 (2018).
13. Talhaoui, I. *et al.* Poly(ADP-ribose) polymerases covalently modify strand break termini in DNA fragments in vitro. *Nucleic Acids Res.* **44**, 9279–9295 (2016).
14. Piscotta, F. J., Jeffrey, P. D. & James Link, A. ParST is a widespread toxin–antitoxin module that targets nucleotide metabolism. *Proc. Natl. Acad. Sci. U. S. A.* **116**, 826–834 (2019).
15. Weigele, P. & Raleigh, E. A. Biosynthesis and Function of Modified Bases in Bacteria and Their Viruses. *Chem. Rev.* **116**, 12655–12687 (2016).
16. Rack, J. G. M., Palazzo, L. & Ahel, I. (ADP-ribosyl)hydrolases: Structure, function, and biology. *Genes Dev.* **34**, 263–284 (2020).
17. Kleine, H. *et al.* Substrate-Assisted Catalysis by PARP10 Limits Its Activity to Mono-ADP-Ribosylation. *Mol. Cell* **32**, 57–69 (2008).
18. Suskiewicz, M. J. *et al.* HPF1 completes the PARP active site for DNA damage-induced ADP-ribosylation. *Nature* **579**, 598–602 (2020).
19. Aravind, L., Zhang, D., de Souza, R. F., Anand, S. & Iyer, L. M. The Natural History of ADP-Ribosyltransferases and the ADP-Ribosylation System. in *Endogenous ADP-Ribosylation* (ed. Koch-Nolte, F.) 3–32 (Springer International Publishing, 2015). doi:10.1007/82_2014_414
20. Jørgensen, R., Wang, Y., Visschedyk, D. & Merrill, A. R. The nature and character of the transition state for the ADP-ribosyltransferase reaction. *EMBO Rep.* **9**, 802–809 (2008).
21. Alemasova, E. E. & Lavrik, O. I. Poly(ADP-ribosyl)ation by PARP1: Reaction mechanism and regulatory proteins. *Nucleic Acids Res.* **47**, 3811–3827 (2019).
22. Schlippe, Y. V. & Hedstrom, L. A twisted base? The role of arginine in enzyme-catalyzed proton abstractions. *Arch. Biochem. Biophys.* **433**, 266–278 (2005).
23. Del Arco, J. *et al.* Reaction mechanism of nucleoside 2′-deoxyribosyltransferases: Free-energy landscape supports an oxocarbenium ion as the reaction intermediate. *Org. Biomol. Chem.* **17**, 7891–7899 (2019).

24. Boshoff, H. I. M., Reed, M. B., Barry, C. E. & Mizrahi, V. DnaE2 polymerase contributes to in vivo survival and the emergence of drug resistance in Mycobacterium tuberculosis. *Cell* **113**, 183–193 (2003).

25. Caminero, J. A. *et al.* Epidemiological evidence of the spread of a Mycobacterium tuberculosis strain of the Beijing genotype on Gran Canaria Island. *Am. J. Respir. Crit. Care Med.* **164**, 1165–1170 (2001).

26. St-Pierre, F. *et al.* One-step cloning and chromosomal integration of DNA. *ACS Synth. Biol.* **2**, 537–541 (2013).

27. Singh, A. K. *et al.* Investigating essential gene function in Mycobacterium tuberculosis using an efficient CRISPR interference system. *Nucleic Acids Res.* **44**, e143 (2016).

28. Guzman, L. M., Weiss, D. S. & Beckwith, J. Domain-swapping analysis of FtsI, FtsL, and FtsQ, bitopic membrane proteins essential for cell division in Escherichia coli. *J. Bacteriol.* **179**, 5094–5103 (1997).

29. Savitsky, P. *et al.* High-throughput production of human proteins for crystallization: The SGC experience. *J. Struct. Biol.* **172**, 3–13 (2010).

30. Lawarée, E. *et al.* DNA ADP-Ribosylation Stalls Replication and Is Reversed by RecF-Mediated Homologous Recombination and Nucleotide Excision Repair. *Cell Rep.* **30**, 1373–1384 (2020).